

# Field-angle Resolved Flux-flow Resistivity as a Phase-sensitive Probe of Unconventional Cooper Pairing

Yoichi Higashi,<sup>1</sup> Yuki Nagai,<sup>2</sup> Masahiko Machida,<sup>2</sup> and Nobuhiko Hayashi<sup>3</sup>

<sup>1</sup>*Department of Mathematical Sciences, Osaka Prefecture University,  
1-1 Gakuen-cho, Naka-ku, Sakai 599-8531, Japan*

<sup>2</sup>*CCSE, Japan Atomic Energy Agency, 5-1-5 Kashiwanoha, Kashiwa, Chiba 277-8587, Japan*

<sup>3</sup>*Nanoscience and Nanotechnology Research Center (N2RC),  
Osaka Prefecture University, 1-2 Gakuen-cho, Naka-ku, Sakai 599-8570, Japan*

(Dated: June 22, 2018)

We theoretically investigate the applied magnetic field-angle dependence of the flux-flow resistivity  $\rho_f(\alpha_M)$  for a uniaxially anisotropic Fermi surface.  $\rho_f$  is related to the quasiparticle scattering rate inside a vortex core, which reflects the sign change in the superconducting pair potential. We find that  $\rho_f(\alpha_M)$  is sensitive to the sign change in the pair potential and has its maximum when the magnetic field is parallel to the gap-node direction. We propose the measurement of the field-angle dependent oscillation of  $\rho_f(\alpha_M)$  as a phase-sensitive field-angle resolved experiment.

PACS numbers: 74.20.Rp, 74.25.Op, 74.25.nm,

## I. INTRODUCTION

It is of great importance to elucidate the symmetry of a superconducting pair potential is of great importance when studying the Cooper pairing mechanism in unconventional superconductors (SCs).

The pair potential is composed of spin and orbital wave functions. The orbital wave function is characterized by its amplitude and phase (sign of the wave function).

In the past decade, experimental techniques for the field-angle resolved specific heat and thermal conductivity measurements have developed to identify the Cooper pairing symmetry in various superconducting systems.<sup>1</sup> These angle-resolved measurements are powerful techniques that can detect the anisotropy of the pair potential amplitude. The theory proposed by Vorontsov and Vekhter has successfully explained these experiments for CeCoIn<sub>5</sub> assuming *d*-wave Cooper pairing.<sup>2</sup> However, these field-angle resolved experiments cannot probe the sign change in the pair potential. That is, they are not phase-sensitive probes. In addition to detecting the anisotropy of the pair potential, it is crucial to probe the phase of the Cooper pair in order to discriminate unconventional SCs, including iron-based SCs, from conventional ones.

Until now, only a few phase-sensitive probes have been developed and succeeded, e.g., the half-flux quantum observation in the tricrystal geometry by a scanning SQUID (superconducting quantum interference device) microscope,<sup>3</sup> and detecting the quasiparticle interference pattern by scanning tunneling spectroscopy (STS).<sup>4</sup> Another phase-sensitive probe is measuring bound states at an interface by point-contact spectroscopy or STS experiments. If both sides of a SC/SC junction are of the same pair potential amplitude but with opposite signs, the quasiparticle (QP) path through the interface acquires a  $\pi$  phase shift and generating bound states around the interface. This situation is similar to a vortex line in super-

conductors. However, there is the difficulty of fabricating a junction in terms of nono-structured processing techniques. Actually, the phase-sensitive test using SC/SC junctions succeeds only for cuprate superconductors.<sup>5</sup> In addition to these existing experiments, a new phase-sensitive test is highly desired.

In this paper, we propose a new experiment that can detect the phase (sign-change) of the pair potential free from fabricating a SC/SC junction. This is the great advantage of the phase-sensitive test proposed in the present work. We theoretically study the in-plane field-angle dependence of the flux-flow resistivity  $\rho_f(\alpha_M)$  for typical gap functions and Fermi surface (FS). From our numerical calculations, we show that the phase-sensitive QP scattering inside a vortex core leads to different behavior of  $\rho_f(\alpha_M)$  between conventional and unconventional Cooper pairing. In addition, we show that  $\rho_f(\alpha_M)$  has its maximum when the applied magnetic field is parallel to the gap-node directions. Our results show that the field-angle dependence of the flux-flow resistivity can detect both the sign change of the pair potential and the direction of the gap nodes.

## II. FLUX-FLOW RESISTIVITY AND QUASIPARTICLE SCATTERING RATE

The flux-flow resistivity  $\rho_f$  is dominated by the quasiparticle within a vortex core. We assume the system belongs to the moderately clean regime, in which there are two important contributions to  $\rho_f$ . One is the QP scattering rate  $\Gamma$  inside a vortex core, and the other is the momentum-dependent quantum level spacing of the vortex bound states  $\omega_0(\mathbf{k}_F)$ .<sup>6,7</sup> Here, the QP scattering is due to non-magnetic impurities randomly distributed in the system.

We attribute the flux-flow resistivity  $\rho_f$  to the energy dissipation of the vortex bound states due to the impurity scattering inside a vortex core.<sup>8</sup>  $\rho_f$  is characterized by the

two quantities mentioned above,<sup>6,7</sup>

$$\rho_f(T) \propto \frac{\Gamma_n}{\Delta_0} \left[ \frac{1}{\nu_0} \int \frac{dS_F}{|\mathbf{v}_F(\mathbf{k}_F)|} \frac{\omega_0(\mathbf{k}_F)}{\Delta_0} \frac{\Gamma_n}{\Gamma(\varepsilon = k_B T, \mathbf{k}_F)} \right]^{-1}, \quad (1)$$

where  $\Gamma_n$  is the impurity scattering rate in the normal state and  $\Delta_0$  is the bulk amplitude of the pair potential. We assume that the temperature  $T$  dependence of  $\rho_f$  comes predominantly from  $\Gamma$  with the QP energy  $\varepsilon = k_B T$ . Here, we have made a rough estimate. Actually, the QPs distributed with the energy width  $\Delta\varepsilon \sim k_B T$  contribute to  $\Gamma$ . The total density of states on a FS is  $\nu_0 = \int dS_F / |\mathbf{v}_F(\mathbf{k}_F)|$ , with  $dS_F = |\mathbf{k}_F(\phi_k, \theta_k)|^2 \sin \theta_k d\phi_k d\theta_k$  being an area element on the FS, the Fermi velocity  $\mathbf{v}_F(\mathbf{k}_F) = \nabla_{\mathbf{k}} \epsilon(\mathbf{k})|_{\mathbf{k}=\mathbf{k}_F}$ , and the Fermi wave vector  $\mathbf{k}_F = |\mathbf{k}_F(\phi_k, \theta_k)|(\bar{\mathbf{a}} \cos \phi_k \sin \theta_k + \bar{\mathbf{b}} \sin \phi_k \sin \theta_k + \bar{\mathbf{c}} \cos \theta_k)$ .  $\epsilon(\mathbf{k})$  is the energy dispersion of electrons.  $\phi_k$  ( $\theta_k$ ) is the azimuthal (polar) angle on the FS.  $\bar{\mathbf{a}}$ ,  $\bar{\mathbf{b}}$ , and  $\bar{\mathbf{c}}$  denote orthogonal unit vectors spanning crystal coordinates. We use the unit system in which  $\hbar = 1$ .

The momentum-dependent inter-level spacing of the vortex bound states  $\omega_0(\mathbf{k}_F)$  is obtained analytically as<sup>9,10</sup>  $\omega_0(\mathbf{k}_F) = 2|d(\mathbf{k}_F)|^2 \Delta_0^2 / (|\mathbf{k}_{F\perp}| |\mathbf{v}_{F\perp}(\mathbf{k}_F)|)$  using the quasiclassical Green's function method and the Kramer-Pesch approximation.<sup>11,12</sup>  $d(\mathbf{k}_F)$  indicates the anisotropy of pair potential and the vector with  $\perp$  denotes the vector component projected onto the plane perpendicular to  $\mathbf{H}$ . We treat the non-magnetic impurity scattering by means of the Born approximation.<sup>8,13</sup> The quasiparticle scattering rate for the QPs with the energy  $\varepsilon$  inside a vortex core is obtained as<sup>12,14</sup>

$$\frac{\Gamma(\varepsilon)}{\Gamma_n} = \left\langle \left\langle \frac{\Gamma(\mathbf{k}_F, \mathbf{k}'_F, \varepsilon)}{\Gamma_n} \right\rangle_{\text{FS}'} \right\rangle_{\text{FS}}, \quad (2)$$

$$\frac{\Gamma(\mathbf{k}_F, \mathbf{k}'_F, \varepsilon)}{\Gamma_n} = \frac{\pi}{2} C(\mathbf{k}_F, \mathbf{k}'_F) D(\mathbf{k}_F, \mathbf{k}'_F) F(\varepsilon, \mathbf{k}_F, \mathbf{k}'_F), \quad (3)$$

$$C(\mathbf{k}_F, \mathbf{k}'_F) = 1 - \text{sgn}[d(\mathbf{k}_F)d(\mathbf{k}'_F)] \cos \Theta, \quad (4)$$

$$D(\mathbf{k}_F, \mathbf{k}'_F) = \frac{1}{|\sin \Theta|}, \quad (5)$$

$$F(\varepsilon, \mathbf{k}_F, \mathbf{k}'_F) = \frac{|\mathbf{v}_{F\perp}(\mathbf{k}'_F)| |d(\mathbf{k}_F)|}{|\mathbf{v}_{F\perp}(\mathbf{k}_F)| |d(\mathbf{k}'_F)|} e^{-u(s_0, \mathbf{k}_F)} e^{-u(s'_0, \mathbf{k}'_F)}. \quad (6)$$

Here,  $\langle \dots \rangle_{\text{FS}} \equiv (1/\nu_0) \int dS_F \dots / |\mathbf{v}_F(\mathbf{k}_F)|$ ,  $\Theta(\mathbf{k}_F, \mathbf{k}'_F) \equiv \theta_v(\mathbf{k}_F) - \theta_{v'}(\mathbf{k}'_F)$  for the scattering angle [see Fig. 1].  $\Gamma$  has the decay factor  $\exp[-u(s_0, \mathbf{k}_F)]$  with  $u(s_0, \mathbf{k}_F) = (2|d(\mathbf{k}_F)|/|\mathbf{v}_{F\perp}(\mathbf{k}_F)|) \int_0^{|s_0|} ds' \tilde{\Delta}(s')$ . We adopt  $\tilde{\Delta}(s') = \Delta_0 \tanh(s'/\xi_0)$  as the spatial variation of the pair potential. The coherence length is defined by  $\xi_0 = v_{F\perp}/(\pi\Delta_0)$  with  $v_{F\perp} \equiv \langle |\mathbf{v}_{F\perp}(\mathbf{k}_F)| \rangle_{\text{FS}}$ . Here, we define the field-angular dependent effective coherence length for the later discussions as

$$\xi_{\text{eff}}(\mathbf{k}_F) = |\mathbf{v}_{F\perp}(\mathbf{k}_F)| / [|\Delta_0 d(\mathbf{k}_F)|]. \quad (7)$$

This length scale  $\xi_{\text{eff}}(\mathbf{k}_F)$  characterizes the size of the bound states of the QP with the momentum  $\mathbf{k}_F$ . Figure 1

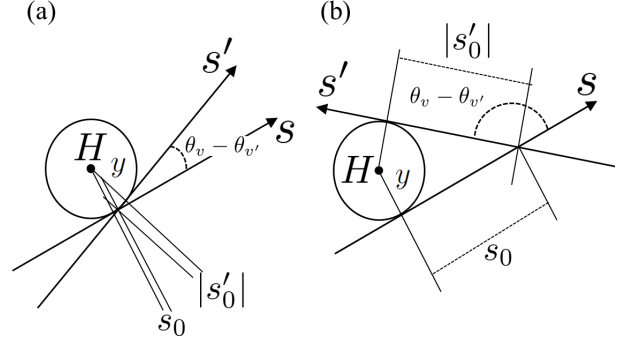


FIG. 1. The schematic figures of (a) the forward scattering and (b) the backward scattering in the vicinity of a vortex.  $s$  and  $s'$  indicate the QP trajectory before and after scattering, respectively.

shows the QP trajectories on the plane perpendicular to the magnetic field  $\mathbf{H}$ . The quantities with a prime are those after scattering.  $s_0$  and  $|s'_0|$  denote the length between the point that is the nearest from the vortex center on the QP trajectory and the scattering point.<sup>12,14</sup>

### III. SYSTEM

In this study, we consider the case in which  $\mathbf{H}$  is applied parallel to the  $a$ - $b$  plane and rotated. The field angle measured from  $a$  axis is  $\alpha_M$ . Here,  $a$ ,  $b$ , and  $c$  are crystal axes. When calculating the dependence of  $\rho_f$  on the magnetic field angle  $\alpha_M$ , we need a coordinate system fixed to  $\mathbf{H}$  which is spanned by  $\bar{\mathbf{a}}_M$ ,  $\bar{\mathbf{b}}_M$ , and  $\bar{\mathbf{c}}_M$  (vortex coordinate system). Here, these axes are orthogonal unit vectors with  $\bar{\mathbf{c}}_M$  set parallel to  $\mathbf{H}$  ( $\bar{\mathbf{c}}_M \parallel \mathbf{H}$ ).  $\mathbf{v}_{F\perp}$ ,  $\theta_v$ , and those with a prime are defined in the vortex coordinates. However,  $\mathbf{k}_F$  and  $\mathbf{k}'_F$  are identified by  $(\phi_k, \theta_k)$  on a FS in the crystal coordinates spanned by  $\bar{\mathbf{a}}$ ,  $\bar{\mathbf{b}}$  and  $\bar{\mathbf{c}}$ , which characterize the crystal axes. In order to calculate the field-angle  $\alpha_M$  dependence of  $\rho_f$ , we need to derive the relation between  $\mathbf{v}_{F\perp}$ ,  $\theta_v$ , and  $\mathbf{v}_F$ ,  $\theta_k$ <sup>14</sup>. Then, the component of  $\mathbf{v}_F(\mathbf{k}_F)$  projected onto the plane perpendicular to  $\mathbf{H}$  is finally obtained as

$$|\mathbf{v}_{F\perp}(\phi_k, \theta_k)| = |\mathbf{v}_F(\phi_k, \theta_k)| \Omega(\phi_k, \theta_k), \quad (8)$$

$$\Omega(\phi_k, \theta_k) = \sqrt{\cos^2 \theta_k + \sin^2(\phi_k - \alpha_M) \sin^2 \theta_k}, \quad (9)$$

$$\cos \theta_v(\phi_k, \theta_k) = \frac{-|\mathbf{v}_F(\phi_k, \theta_k)|}{|\mathbf{v}_{F\perp}(\phi_k, \theta_k)|} \cos \theta_k, \quad (10)$$

$$\sin \theta_v(\phi_k, \theta_k) = \frac{|\mathbf{v}_F(\phi_k, \theta_k)|}{|\mathbf{v}_{F\perp}(\phi_k, \theta_k)|} \sin(\phi_k - \alpha_M) \sin \theta_k. \quad (11)$$

Thus, the relation between the vortex coordinate and the crystal coordinate is derived. Here we give the expression of the projected Fermi velocity for an arbitrary anisotropic FS (see Ref. 15 for the expression for a uniaxially anisotropic FS). We have now reached the position

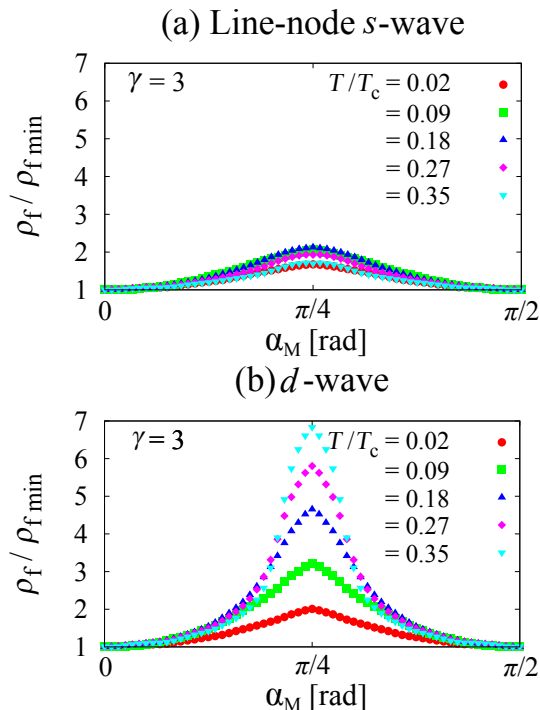


FIG. 2. (Color online) Field-angle ( $\alpha_M$ ) dependence of the flux-flow resistivity  $\rho_f$  in the case of (a) line-node  $s$ -wave and (b)  $d$ -wave pair for a spheroidal FS ( $\gamma = 3$ ). Each curve indicates different temperature. The vertical axis is normalized by the minimum value of  $\rho_{f \text{ min}}$  for each plot.

where we can perform the numerical integration on FS and calculate the field-angle dependence of Eq. (1).

We consider the following two types of the simple pair potential model. One is a line-node  $s$ -wave pair:  $d(\mathbf{k}_F) = |\cos 2\phi_k| \sin^2 \theta_k$ . The other is a  $d_{x^2-y^2}$ -wave one:  $d(\mathbf{k}_F) = \cos 2\phi_k \sin^2 \theta_k$ . Each one has gap nodes from the north pole of the FS to the south one in the  $\phi_k = (1 + 2n)\pi/4$  [rad] directions (gap-node directions) with  $n = 0, 1, 2, 3$ .  $\phi_k = n\pi/2$  [rad] directions correspond to anti-node directions. In the momentum space, these two pair potentials have the same anisotropy in their amplitude  $|d(\mathbf{k}_F)|$ . However, only the  $d$ -wave pair has the sign change and the  $s$ -wave pair does not.

Our calculations are performed for a uniaxially anisotropic FS with the mass anisotropy parameter  $\gamma = \sqrt{m_c/m_{ab}}$ <sup>15</sup>.  $m_c$  and  $m_{ab}$  are masses characterizing charge transport along the  $c$ -axis and within the  $a-b$  plane, respectively.

## IV. RESULTS

### A. Field-angular dependence of flux-flow resistivity

We show numerical results for a uniaxially anisotropic FS with  $\gamma = 3$ . In Fig. 2, we show the field-angle de-

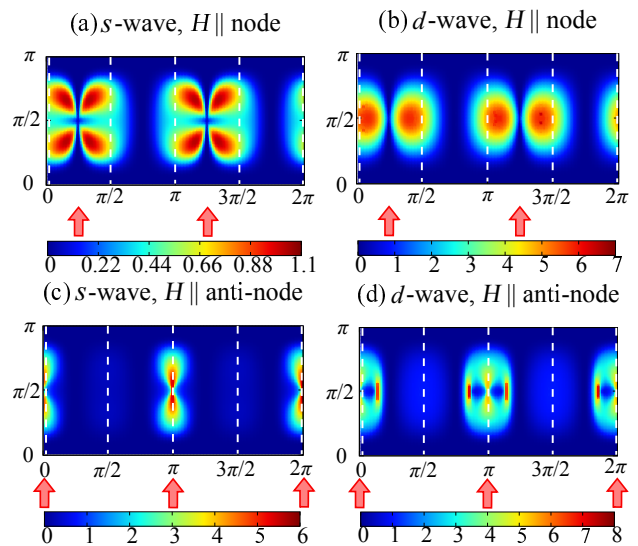


FIG. 3. (Color online)  $\mathbf{k}_F$  dependence of  $\Gamma$  in the case of (a) the line-node  $s$ -wave pair when  $\mathbf{H} \parallel$  the gap-node direction, (b)  $d$ -wave pair when  $\mathbf{H} \parallel$  the gap-node direction, (c) the line-node  $s$ -wave pair when  $\mathbf{H} \parallel$  the anti-node direction and (d)  $d$ -wave pair when  $\mathbf{H} \parallel$  the anti-node direction on a spheroidal FS ( $\gamma = 3$ ). The quasiparticle energy  $\varepsilon$  is set to  $0.2\Delta_0$  in each plot. The vertical and horizontal axes denote the polar angle  $\theta_k$  and the azimuthal angle  $\phi_k$  respectively. The dotted lines indicate the anti-node directions. The field directions are indicated by arrows.

pendence of the flux-flow resistivity  $\rho_f(\alpha_M)$  for the two pair potential models. As shown in Fig. 2(a), in the case of the line-node  $s$ -wave pair, a broad maximum appears when  $\mathbf{H}$  is applied parallel to the gap-node direction ( $\alpha_M = \pi/4$ ). Note that the field-angle dependence of the QP scattering rate  $\Gamma(\alpha_M)$  has its minimum when  $\mathbf{H}$  is parallel to the node direction.<sup>14,15</sup> The oscillation amplitude of  $\rho_f(\alpha_M)$  remains small compared with the  $d$ -wave case when the temperature  $T$  is increased.  $\rho_f(\alpha_M)$  has little dependence on  $T$  in the case of the line-node  $s$ -wave pair.

On the other hand, in the  $d$ -wave case [Fig. 2(b)], a sharp maximum appears when  $\mathbf{H}$  is applied to the gap-node direction. The oscillation amplitude grows with increasing  $T$  in contrast to the line-node  $s$ -wave pair. This behavior indicates that the peak of  $\rho_f(\alpha_M)$  has a strong temperature dependence in the  $d$ -wave case.

The field-angle dependence of  $\rho_f$  is quite contrasting between the line-node  $s$ -wave pair and the  $d$ -wave one. One would question what the reason for this prominent difference is. We consider that this difference comes from whether there is a sign change in the pair potential or not.

### B. Quasiparticle scattering on the Fermi surface

First, we list the characteristics of the  $\mathbf{k}_F$  dependence of the QP scattering rate  $\Gamma(\mathbf{k}_F)/\Gamma_n$ .  $\Gamma(\mathbf{k}_F)/\Gamma_n$  is ob-

TABLE I. The QP scattering types.

	Forward scattering $\Theta(\mathbf{k}_F, \mathbf{k}'_F) = 0$	Backward scattering $\Theta(\mathbf{k}_F, \mathbf{k}'_F) = \pi$
sign-conserved	suppressed	small
sign-reversed	enhanced	suppressed

tained by integrating Eq. (3) with respect to  $\mathbf{k}'_F$ . Next, we explain the behavior of  $\Gamma(\alpha_M)$ .

To clarify why  $\rho_f(\alpha_M)$  behaves contrastingly between the two pair potential models, we investigate the  $\mathbf{k}_F$  dependence of  $\Gamma$  first.  $\Gamma(\mathbf{k}_F)/\Gamma_n$  indicates which QPs are easy to be scattered on the FS. We find the following characteristics of the QP scattering: (i) The QPs in the vicinity of the anti-node direction predominantly contribute to  $\Gamma$ , as seen in Figs. 3(a)–3(d).  $\Gamma(\mathbf{k}_F)/\Gamma_n$  has a higher value around anti-node directions (see around the dotted lines). We describe the physical picture for this characteristics as follows. The QPs flowing in the direction of the gap nodes feel the small amplitude of the pair potential [i.e., small  $\Delta_0|d(\mathbf{k}_F)|$ ] even in the bulk. Then,  $\xi_{\text{eff}}(\mathbf{k}_F) = |\mathbf{v}_{F\perp}|/[\Delta_0|d(\mathbf{k}_F)|]$  becomes large. Thus a vortex core spreads out effectively because of the large effective coherence length  $\xi_{\text{eff}}$ , and the QP wave function extends outside a vortex core. The wave function is damped exponentially by a factor  $\exp[-u(s_0, \mathbf{k}_F)]$  and  $\Gamma$  for the QPs in the node directions becomes small [see Eq. (6)]. On the other hand, the QPs flowing in the direction of the anti-nodes feel the full amplitude of the pair potential ( $\Delta_0$ ). Then, a vortex core gets small effectively because  $\xi_{\text{eff}}$  becomes small. Hence, the QP wave function is strongly localized inside a vortex core and scattered inside it, giving a large contribution to  $\Gamma$ . (ii) There is the tendency that the QPs in the direction of  $\mathbf{H}$  are easy to be scattered. As seen in Figs. 3(a) and 3(b), this property of the QP scattering is confirmed by the fact that the weight of  $\Gamma$  shifts a bit toward the field direction. The tendency is obvious in Figs. 3(c) and 3(d). The reason why the QPs have above tendency is because  $|\mathbf{v}_{F\perp}(\mathbf{k}_F)|$  of the QPs in the field direction is small and the contribution to  $\Gamma$  becomes large [see Eq. (6) and Fig. 5]. (iii) The other contribution to  $\Gamma$  is expressed by the coherence factor  $C(\mathbf{k}_F, \mathbf{k}'_F)$ ,<sup>12</sup> which reflects the sign of the pair potential in Eq. (4). This characteristic is discussed in detail in Ref. 12. Here we summarize their results (i.e., the dependence of  $\Gamma$  on the QP scattering types) in Table I.

## V. FIELD-ANGULAR DEPENDENCE OF THE QUASIPARTICLE SCATTERING RATE

First of all, we consider  $\Gamma$ , which is a part of the contribution to  $\rho_f$  as shown in Eq.(1). In the case of the line-node  $s$ -wave pair, taking into account the characteristics of the QP scattering (i) – (iii), we can explain

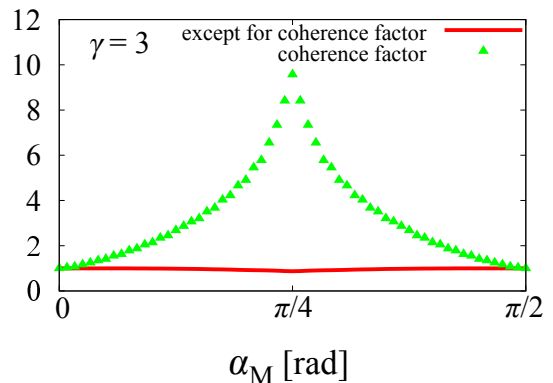


FIG. 4. (Color online) Field-angle ( $\alpha_M$ ) dependences of the part of  $\Gamma$  containing the coherence factor and the other part of it for the  $d$ -wave pair with the spheroidal FS. The vertical axis is normalized by the minimum value.

qualitatively the behavior of  $\Gamma(\alpha_M)$ . In the line-node  $s$ -wave pair,  $\Gamma(\alpha_M)$  has its minimum when  $\mathbf{H}$  is applied to the gap-node direction<sup>14,15</sup>. In this case, according to the factor (iii), the effect of the coherence factor on  $\Gamma(\mathbf{k}_F)/\Gamma_n$  is small. In addition, in the line-node  $s$ -wave pair, we confirmed that the coherence factor has no field-angle dependence. Hence, we can neglect the factor (iii) in the line-node  $s$ -wave pair.

When  $\mathbf{H}$  is parallel to the gap-node direction, the weight of  $\Gamma(\mathbf{k}_F)/\Gamma_n$  shifts toward the field direction (i.e., the gap-node direction) due to the factor (ii). Therefore, the QPs around the gap node become easier to be scattered. However, according to the factor (i), the contribution of the QPs in the vicinity of the gap nodes to  $\Gamma(\mathbf{k}_F)/\Gamma_n$  is small. Hence, the large contribution to  $\Gamma(\mathbf{k}_F)/\Gamma_n$  due to the factor (ii) gets small due to the factor (i).

On the other hand, when  $\mathbf{H}$  is parallel to the anti-node direction, the QPs in the direction of  $\mathbf{H}$  (i.e., the anti-node direction), which have small  $\mathbf{v}_{F\perp}(\mathbf{k}_F)$ , can give a large contribution to  $\Gamma(\mathbf{k}_F)/\Gamma_n$  due to the factor (ii). In this case, contrary to the case of  $\mathbf{H}$  parallel to the node direction,  $\Gamma$  remains large due to the factor (i). As a result of the above consideration, the minimum of  $\Gamma(\alpha_M)$  appears when  $\mathbf{H}$  is parallel to the gap-node direction.

In the case of the  $d$ -wave pair, the backward scattering is suppressed (see Table I) since the coherence factor becomes zero and the scattering point is far from the vortex core. However, the forward scattering with the sign change of pair potential is enhanced (see Table I). So the coherence factor gives the large contribution to  $\Gamma(\mathbf{k}_F)/\Gamma_n$ . In Fig. 4, we show the field-angle dependences of  $\langle\langle C(\mathbf{k}_F, \mathbf{k}'_F)D(\mathbf{k}_F, \mathbf{k}'_F) \rangle\rangle_{\text{FS}'\text{FS}}$ , which is the part of  $\Gamma(\varepsilon)/\Gamma_n$  containing the coherence factor  $C(\mathbf{k}_F, \mathbf{k}'_F)$ . We also calculate the field-angle dependences of  $\langle\langle F(\varepsilon, \mathbf{k}_F, \mathbf{k}'_F) \rangle\rangle_{\text{FS}'\text{FS}}$ , which does not contain the coherence factor. When  $\mathbf{H}$  is parallel to the node direction,  $\langle\langle C(\mathbf{k}_F, \mathbf{k}'_F)D(\mathbf{k}_F, \mathbf{k}'_F) \rangle\rangle_{\text{FS}'\text{FS}}$  shows a sharp maxi-

mum. On the other hand,  $\langle\langle F(\varepsilon, \mathbf{k}_F, \mathbf{k}'_F) \rangle\rangle_{\text{FS}'/\text{FS}}$  shows little field-angle dependence. This sharp maximum reproduces the behavior of  $\Gamma(\alpha_M)$  in the  $d$ -wave case.<sup>14,15</sup>

Let us explain the physical picture of the QP scattering rate in the  $d$ -wave case. First of all, we should note that the intensity of the forward scattering is the important factor of the QP scattering around a vortex, since the forward scatterings occur when the scattering point is near the vortex center (i.e., the QP scattering occurs inside a vortex core), as shown in Fig. 1. Thus, we consider the field-angle dependence of the intensity of the forward scattering. We note that the intensity of the forward scattering becomes larger upon decreasing the effective coherence length  $\xi_{\text{eff}}(\mathbf{k}_F)$ . The effective coherence length  $\xi_{\text{eff}}(\mathbf{k}_F)$  defined by Eq. (7) is proportional to the projected Fermi velocity  $\mathbf{v}_{F\perp}(\mathbf{k}_F)$  and is inversely proportional to the amplitude of a pair potential  $\Delta_0|d(\mathbf{k}_F)|$ . The minimum effective coherence length is zero when the Fermi velocity  $\mathbf{v}_F(\mathbf{k}_F)$  is parallel to  $\mathbf{H}$  [i.e.,  $\mathbf{v}_{F\perp}(\mathbf{k}_F)$  becomes zero]. As shown in Fig. 3, the intensity of  $\Gamma(\mathbf{k}_F)$  becomes large in the region where  $\mathbf{v}_{F\perp}(\mathbf{k}_F)$  becomes small. This is the reason for the factor (ii).

The most important factor of the intensity of the forward scattering is the factor (iii). As shown in Table I, the sign-conserved forward scattering is suppressed even when the effective coherence length becomes small. Therefore, the sign-reversed forward scatterings with the small effective coherence length dominantly contribute to the QP scattering rate in the  $d$ -wave case. When  $\mathbf{H}$  is parallel to the gap-node direction, we have confirmed numerically that the forward scattering is realized by calculating the contribution of anti-nodal QPs to  $\Gamma(\varepsilon, \mathbf{k}'_F, \alpha_M = \pi/4)$ . As shown in Fig. 5, the forward scattering occurs through the QP scattering in the parallel direction of  $\mathbf{H}$  when  $\mathbf{H}$  is parallel to the gap-node direction. Moreover, this QP scattering process is sign-reversing, since the quasiparticles with  $\mathbf{v}_F$  are scattered across the gap-node perpendicular to  $\mathbf{H}$ . Hence, the sign-reversed forward scattering occurs when  $\mathbf{H}$  is parallel to the gap-node direction even in a single-band superconductor.

On the other hand, when  $\mathbf{H}$  is parallel to the anti-node direction, it was revealed through the same analysis that although the sign-reversed scattering occurs, not only the forward scattering but also the backward scattering occurs. As a result of the above discussion, the quasiparticle scattering rate is enhanced when  $\mathbf{H}$  is parallel to the gap-node direction in the  $d$ -wave case.

## VI. FIELD-ANGULAR DEPENDENCE OF FLUX-FLOW RESISTIVITY

The other contribution to  $\rho_f$  is  $\omega_0(\mathbf{k}_F)$ . When  $\Gamma(\varepsilon, \mathbf{k}_F) = \text{const.}$ , the field angle dependence of  $\omega_0(\mathbf{k}_F)$  for a spheroidal FS is not qualitatively different from that for an isotropic FS.<sup>9</sup> When  $\omega_0(\mathbf{k}_F) = \text{const.}$ ,  $\rho_f(T) \propto \Gamma(\varepsilon = k_B T)$ . In the  $d$ -wave case, the dependence of

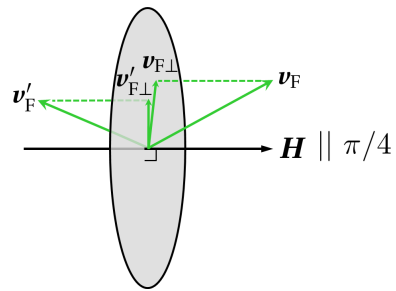


FIG. 5. Schematic figure of the forward QP scattering, which is characterized by the angle between the projections of the Fermi velocities onto the plane perpendicular to an in-plane magnetic field  $\mathbf{H}$ .

$\omega_0(\mathbf{k}_F)$  on the field-angle makes the behavior of  $\Gamma(\alpha_M)$  stand out. As a result,  $\rho_f(\alpha_M)$  has a sharp maximum when  $\mathbf{H}$  is parallel to the gap-node direction. On the other hand, in the  $s$ -wave case, the field angle dependence of  $\omega_0(\mathbf{k}_F)$  makes the oscillation amplitude of  $\Gamma(\alpha_M)$  inverted and  $\rho_f(\alpha_M)$  has its broad maximum when  $\mathbf{H}$  is parallel to the gap-node direction.

## VII. DISCUSSIONS

Finally, we comment on the experimental condition for measuring the flux-flow resistivity under a rotating magnetic field. Our theory is based on the vortex bound states formed inside a vortex core. Therefore, an extremely two-dimensional system, in which a Josephson vortex is formed parallel to the layer, is beyond our theoretical framework. However, we should note that our method can be applied to iron-pnictides, which have a warped cylindrical Fermi surface such as that found in 11-compounds (FeSe or FeTe) and 122-compounds  $[\text{BaFe}_2(\text{As}_{1-x}\text{P}_x)_2]$ , since the angular-resolved specific heat and thermal conductivity measurements have successfully detected the gap minima in  $\text{FeSe}_{0.45}\text{Te}_{0.55}$ <sup>16</sup> and the position of the gap-nodes in  $\text{BaFe}_2(\text{As}_{0.67}\text{P}_{0.33})_2$ ,<sup>17</sup> respectively, under a rotated magnetic field within the basal plane. In layered organic compounds  $\kappa\text{-(ET)}_2\text{Cu(NCS)}_2$ , in-plane field angular dependence of the Josephson-vortex flow resistance has already been measured by Yasuzuka *et al.*,<sup>18</sup> but in a three-dimensional system, measurement of the flux-flow resistivity has not been performed yet. We calculate  $\rho_f(\alpha_M)$  also in the case of the in-plane anisotropic FS.<sup>19</sup> In this case, the behavior of  $\rho_f(\alpha_M)$  is not qualitatively different from that in the isotropic FS case. When considering multiband superconductors such as iron-based superconductors, we need to take into account the contribution from holelike FS to the flux-flow resistivity in addition to that from electronlike FS.<sup>6</sup> In this study, we consider the contribution only from electronlike FS. The multiband effect on the flux-flow resistivity is left for future

study.

### VIII. CONCLUSION

In conclusion, we theoretically studied the in-plane magnetic field-angle dependence of the flux-flow resistivity for a uniaxially anisotropic FS. We showed that the measurement of the flux-flow resistivity changing the field direction within the  $a$ - $b$  plane can detect both the position of the gap nodes and the sign change of the pairing

potential. One can estimate the flux-flow resistivity by means of microwaves. Instead of fabricating a junction, one can obtain the information on the phase of the pair potential by measuring the microwave surface impedance under a rotating magnetic field.

### ACKNOWLEDGMENT

The authors thank T. Okada and S. Yasuzuka for helpful discussions.

- 
- <sup>1</sup> T. Sakakibara, A. Yamada, J. Custers, K. Yano, T. Tayama, H. Aoki, and K. Machida, *J. Phys. Soc. Jpn.* **76**, 051004 (2007); Y. Matsuda, K. Izawa, and I. Vekhter, *J. Phys.: Condens. Matter* **18**, R705 (2006).
- <sup>2</sup> A. B. Vorontsov and I. Vekhter, *Phys. Rev. B* **75**, 224501 (2007); **75**, 224502 (2007).
- <sup>3</sup> C. C. Tsuei, J. R. Kirtley, C. C. Chi, L. S. Yu-Jahnes, A. Gupta, T. Shaw, J. Z. Sun, and M. B. Ketchen, *Phys. Rev. Lett.* **73**, 593 (1994).
- <sup>4</sup> T. Hanaguri, S. Nittaka, K. Kuroki, and H. Takagi, *Science* **328**, 474 (2010).
- <sup>5</sup> D. J. Van Harlingen, *Rev. Mod. Phys.* **67**, 515 (1995); C. C. Tsuei and J. R. Kirtley, *ibid.* **72**, 969 (2000).
- <sup>6</sup> N. B. Kopnin and G. E. Volovik, *Phys. Rev. Lett.* **79** (1997) 1377.
- <sup>7</sup> Yu. G. Makhlin, *Phys. Rev. B* **56** (1997) 11872; N. B. Kopnin, G. E. Volovik, and Ü. Parts, *Europhys. Lett.* **32** 651 (1995); Alan T. Dorsey, *Phys. Rev. B* **46**, 8376 (1992).
- <sup>8</sup> Y. Kato, *J. Phys. Soc. Jpn.* **69** (2000) 3378.
- <sup>9</sup> Y. Higashi, Y. Nagai, M. Machida, and N. Hayashi, *J. Phys: Conf. Ser.* **400**, 022025 (2012).
- <sup>10</sup> G. E. Volovik, *Pis'ma Zh. Eksp. Teor. Fiz.* **58**, 444 (1993) [*JETP Lett.* **58**, 455 (1993)]; **70**, 601 (1999) [**70**, 609 (1999)]; N. B. Kopnin and G. E. Volovik, *ibid.* **64**, 641 (1996) [**64**, 690 (1996)].
- <sup>11</sup> Y. Nagai and N. Hayashi, *Phys. Rev. Lett.* **101** (2008) 097001; Y. Nagai, Y. Ueno, Y. Kato, and N. Hayashi, *J. Phys. Soc. Jpn.* **75** (2006) 104701, and references therein.
- <sup>12</sup> Y. Nagai and Y. Kato, *Phys. Rev. B* **82** (2010) 174507.
- <sup>13</sup> L. J. Buchholtz and G. Zwicknagl, *Phys. Rev. B* **23**, 5788 (1981); E. V. Thuneberg, J. Kurkijärvi, and D. Rainer, *ibid.* **29**, 3913 (1984); N. Hayashi, Y. Kato, and M. Sigrist, *J. Low Temp. Phys.* **139**, 79 (2005).
- <sup>14</sup> Y. Higashi, Y. Nagai, M. Machida, and N. Hayashi, *Physica C* **471**, 828 (2011).
- <sup>15</sup> Y. Higashi, Y. Nagai, M. Machida, and N. Hayashi, *Physica C* **484**, 97 (2013).
- <sup>16</sup> B. Zeng, G. Mu, H. Q. Luo, T. Xiang, I. I. Mazin, H. Yang, L. Shan, C. Ren, P. C. Dai, and H.-H. Wen, *Nat. Commun.* **1**, 112 (2010).
- <sup>17</sup> M. Yamashita, Y. Senshu, T. Shibauchi, S. Kasahara, K. Hashimoto, D. Watanabe, H. Ikeda, T. Terashima, I. Vekhter, A. B. Vorontsov, and Y. Matsuda, *Phys. Rev. B* **84**, 060507(R) (2011).
- <sup>18</sup> S. Yasuzuka, S. Uji, H. Satsukawa, M. Kimata, T. Terashima, H. Koga, Y. Yamamura, K. Saito, H. Akutsu, and J. Yamada, *Physica B* **405**, S288 (2010); S. Yasuzuka, K. Saito, S. Uji, M. Kimata, H. Satsukawa, T. Terashima, and J. Yamada, *J. Phys. Soc. Jpn.* **82**, 064716 (2013).
- <sup>19</sup> Y. Higashi, Y. Nagai, M. Machida, and N. Hayashi, *Phys. Proc.* **45**, 137 (2013).